Design and analysis of multi-section eccentric shaft

Javier Resto, MSME
Associate Professor, PUPR
Department of Mechanical Engineering

Abstract

In this report the preliminary design and analysis of multi-section eccentric shaft to be used on four-rotor Wankel rotary engine is discussed. Only a static analysis was performed due to time constraints. This novel design uses tapered three-sided polygon couplings to connect the different sections of the shaft. The design used Pro/ENGINEER® solid modeler. The shaft size was based on a maximum torque of 400 ft-lb. and a maximum angular velocity of 1,047 rad/sec (10,000 revolutions per minute, rpm). A finite element analysis was performed on the most highly loaded coupling of the shaft using COSMOS/M® finite element analysis system. Solid (brick) elements were used to model the two parts comprising the coupling. Contact (gap) elements were used to model the interface between the two parts of the coupling. The results of the static analysis show that the maximum von Mises stress in the parts is 58,000 psi. The factor of safety based on a minimum yield strength of 217,000 psi for a normalized and tempered 4340 low alloy steel forging is 3.74.

Análisis y diseño de un eje excéntrico de múltiples secciones

Sinopsis

Este artículo presenta el análisis y diseño de un eje excéntrico de múltiples secciones para usarlo en un motor rotativo Wankel de cuatro rotores. Solamente se realizó análisis estático por las limitaciones de tiempo. Este innovador diseño usa acopladores poligonales de tres lados ("three-sided polygon couplings") para conectar las diferentes secciones del eje. El diseño

usó el programa Pro/ENGINEER® . El tamaño del eje se consideró a base de un torque máximo de 400 ft-lb y una velocidad angular de 1047 rad/sec (10,000 revoluciones por minuto, rpm). Se hizo un análisis de elementos finitos en el acoplamiento más cargado del eje con el sistema para análisis de elementos finitos COSMOS/M®. Se usaron elementos sólidos (ladrillo) para modelar las dos partes que comprenden el acoplamiento.También se usaron elementos de contacto (gap) para modelar la interfase entre ambas partes del acoplamiento. Los resultados del análisis estático demuestran que el esfuerzo máximo de von Mises en las piezas es de 58,000 psi. Se consideró un factor de seguridad de 3.74 a base de un rendimiento mínimo de esfuerzos de 217,000 psi para una aleación de acero forjado normalizada y templada 4340 ("low alloy steel").

Introduction

The performance of a Wankel rotary engine can be augmented substantially by increasing its number of rotors. Yamamoto (1968) states the advantages of a multi-rotor rotary engine:

1. Improvement of performance by increasing the total displacement.
2. Reduction in torque fluctuation.
3. Easier balance with inertia force and couple.
4. Capability of increasing the allowable engine speed by reducing the bearing loads and the sliding speed of gas seals in case the total displacement is kept the same.

Several methods have been used in the past to accomplish this task. One of these methods involves splitting of the phasing gears and main bearings. Another method uses a segmented eccentric shaft. The purpose of this report is to present the results of the preliminary design and analysis of an eccentric shaft for a four-rotor Wankel rotary engine. This design uses a split type eccentric shaft with sections connected by three-sided tapered polygon couplings. This method of coupling has never been used before for this type of application. A static non-linear finite element analysis using contact elements was performed on the most highly loaded coupling to check the

feasibility of the design.

Wankel engine overview

A rotary engine is defined as an internal combustion engine that performs the four-stroke cycles of intake, compression, expansion and exhaust while the working chamber changes its volume and the moving parts always rotate in the same direction. There are three types of rotary engines: single rotating, oscillatory rotating engine, and planetary rotating engine. A single rotating engine is one in which the rotor rotates at a certain angular velocity and the center of its rotation does not move. The oscillatory engine is an engine in which a number of rotors rotate around the center of rotation by changing their angular velocity and the chamber volume changes as the rotors come close to each other or separate from each other. A planetary rotating engine is one engine in which a rotor rotates by making a planetary motion.

The Wankel rotary engine is a typical example of a planetary rotating engine. In this engine a two-lobe epitrochoid is used on the outer envelope or housing and a three-lobe hypotrochoid is used on the rotor. An internal gear attached to a bore on the rotor meshes with a stationary gear which is concentric with the output shaft and is bolted to one of the side housings. Since the center of the rotor and the center of the output shaft are eccentric to each other, the gas pressure on the rotor translates into rotating power output on the shaft. The working chamber does not make a rotating motion; therefore, gas seals located on the rotor flanks and apexes are used to secure gas tightness in. the working chamber (Ansdale,1968; Norbye, 1972; Yamamoto, 1969).

The Wankel rotary engine has several advantages over the reciprocating piston engine. The most important one is that it does not have any reciprocating parts. Therefore, there is not any unbalance caused by the inertia of reciprocating parts. This means less engine vibration, less mechanical loss, simpler construction and a smaller package. Another advantage is that in the Wankel rotary engine the rotor is the one that opens and closes the intake and exhaust ports; hence, it does not require any complicated valve train to perform this function. This means fewer parts and smaller weight. Another

advantage of the Wankel engine is that there is one combustion cycle per revolution of the output shaft instead of one combustion cycle for every two revolutions as is the case in a reciprocating engine (comparing single rotor rotary engine vs single piston reciprocating engine). This translates into less torque fluctuation for the rotary engine, therefore, a flatter torque curve.

The Wankel rotary engine is intrinsically an engine with very low torque fluctuation, as was mentioned above. This pleasant characteristic can be improved with the addition of multiple rotors. In addition to better torque curve, a multi-rotor engine will have an improved performance by the increase in total displacement of the engine. The multi-rotor arrangement also provides an easier balance of the shaft and will allow an increase in the maximum allowable rpm of the engine by reducing the loading at the bearings and the sliding speed of the sealing elements when the total engine displacement is kept unchanged.

In order to be able to make an in-line multi-rotor Wankel rotary engine of more than two rotors, additional stationary gears and main bearings are needed for the rotors located in the middle section of the eccentric shaft. This can be accomplished by two different methods. One is to split both the stationary gears and main bearings located at the middle sections of the shaft. The other method requires a multi-section eccentric shaft that can be assembled into the stationary gears and main bearings. Figures 1 and 2 illustrate the split type and multi-section types of construction, respectively (Norbye, 1972; Yamamoto, 1969).

The multi-section eccentric was chosen as the preferred method for this study. To accomplish this task, we used three-sided tapered polygon couplings to connect the shaft sections together.

Design of multi-section shaft

Requirements are the heart of every design. Without them the product being designed does not have any reason to be. The requirements imposed on the design of this multi-section shaft are:

1. The maximum number of parts from existing engines are going to be used. The rotor housings, side housings, stationary gear and main bearing assemblies flywheel, and pulleys from a Mazda® two-rotor engine is to be used.
2. Since commercial parts are going to be used, the shaft must be designed in such a way that the assembly and disassembly of the engine are not compromised. The type of coupling used must facilitate the longitudinal and angular positioning of the sections according to overall engine envelope.
3. The shaft must have enough torsional stiffness to avoid high angular distortion. This characteristic will guarantee high power transfer efficiency. Zero initial backlash in the connection is also required to avoid the introduction of any sort of impact loading into the power train.
4. The shaft assembly should be able to transmit a maximum torque of 400 ft-lb at 10,000 rpm.

Three different concepts for coupling the sections of the shaft were evaluated. The first concept uses a spline to connect the sections. Some of the advantages of this type of connection are low cost, ease of manufacture, and availability. The disadvantages are propensity to failure because of stress concentration in the teeth, low concentricity and low clearance control. Other disadvantages are that the part has to be hardened after final machining, which can cause distortion in the part, and the fact that it does not provide good control of angular position or backlash.

The second and third concepts are a straight three-sided polygon coupling and a tapered three-sided polygon coupling. These two types of couplings have some advantages in common. The advantages are higher shear strength, which translates into higher torque carrying capacity and shorter connections; better concentricity; zero stress raisers and angular positioning accuracy within five seconds. The tapered three-sided polygon has one advantage over the straight three-sided polygon that makes it preferable for the application under study. This advantage is that it offers zero backlash without the use of press or interference fit. This characteristic makes the multi-section shaft much easier

to assemble and disassemble.

After a careful analysis of the advantages and disadvantages of the all three concepts, it was decided that the tapered three-sided polygon coupling has the characteristics that best fit the parts being designed. The characteristic of being able to have zero backlash without interference fit makes this option better than the straight three-sided polygon coupling. The characteristics of higher shear strength, better concentricity, zero stress raisers, and excellent angular position control make the tapered polygon coupling a better connection than the spline.

The preliminary design of the shaft sections can be seen in figures 3 through 8. Figure 3 depicts the front section of the shaft. The figure also shows the cylindrical section with a keyway where the distributor gear, the oil pump drive and the pulley assembly are going to be installed. The female polygon coupling can be seen at the right side of the picture. An internal undercut was added at the back of the bore in order to facilitate the manufacturing of the polygon. This undercut reduces the wear on the grinding wheel and reduces the manufacturing time. The holes and the grove for bearing lubrication are placed on the journal surfaces. It should be mentioned that the location and size of the journals were kept the same as in the Mazda® rotary engine. Figures 4 and 5 depict the center sections of the shaft. These two sections have both female and male parts of the coupling machine on them. The oiling holes where located at areas where the stress are thought to be lower. Undercuts were included at the back of the bore of each female coupling. Generous fillets were included to minimize stress concentration at every shaft shoulder. The last section of the shaft can be seen in figure 6. The same design principles used on the first three sections were used for the design of this section, i.e., generous fillet radii, lubrication holes located at low stress areas, etc. The right side of this shaft was designed to match the attachment requirements for the flywheel used on the commercially available engine. The flywheel is attached to the tapered cylindrical shaft by a semicircular key and keyway and held in place by a nut. The tie bolt used to hold all the sections together is shown in figure 8. The bolt has a snug fit at both front and rear ends. The ends should be sealed in order to avoid any lubricant leak. The bolt

has a slotted head to be able to compress the whole assembly using the nut at the front end of the shaft.

Figure 7 shows an assembly of the shaft with all the components in it. The eccentric sections are clocked 90 degrees clockwise from front to rear. All sections and tie bolt, depicted in figure 8, are made out of 4340 low alloy steel forgings. The specified mechanical properties for this material (Brown, 1993):

- Condition: normalized and tempered
- Yield strength: 217,000 psi (minimum)
- Ultimate tensile strength: 260,000 psi (minimum)
- Hardness: 269 BHN

This is a material with very good mechanical properties that has been used on shafts for high performance applications for many years. The weight of the assembled shaft shown in figure 7 is about 22 lb.

Finite element analysis

Since all the connections in the shaft have the same dimensions and are made out of the same material, the coupling with the highest loading was chosen as the one to be analyzed. The coupling between sections 3 and 4 of the shaft is the only one that will have to withstand all the torque coming from the four rotors. This is because it is the connection closest to the point where the power train attaches to the engine. As mentioned before, it is assumed that the engine is producing 400 ft-lb of torque at 10,000 rpm; therefore this is the loading to be used in the analysis. The Young's modulus of elasticity for the material is 29.5 psi and the Poisson's ratio is 0.30. The temperature is assumed to be 200° F. At this temperature the properties of the material are practically the same as the ones at room temperature.

The connection was modeled as two separate sections coming in contact with each other. The two contact surfaces, the internal and external polygon surfaces on the male and female parts, respectively, were created from the same geometry. Therefore, an offset of 1 mm (.0394 in) was used to separate

the two surfaces. This means that the gap created between the two parts has to be closed by the applied loads before any torque can be transmitted. COSMOS/M® finite element analysis system was used for the analysis. Contact elements were used to model the interface between the two parts. A contact problem is considered as a general case of a gap problem in which the direction of the normal gap force is not fixed and in which the point of contact can change with the application of the load. The convergence of this type of problem depends on an incremental solution where the forces have to be applied gradually. Figure 9 shows the load vs. time line that controls the application of the loads. This line is defined by specifying the load level at different time steps. In order to be able to gradually control the application of the loads, a nonlinear static analysis was performed. This enables the nodes to move slowly on the surface. In this case, the body which moves to make contact is declared the "contactor," while the body which receives the contact is called the "target" (Niazy and Kahyai, 1994).

The sections were meshed by using solid 8-node elements. In order to obtain good bending behavior at least three solid elements were used to model the thickness or cross sections of the parts. The model has areas where the element size looks coarse, but it can be noted in the results that the stress gradient across the models is very smooth; i.e, there is no large stress differential between adjacent elements. Therefore, refinement of the mesh size is not needed in this case. No mesh refinement was used at the structural discontinuities shown in the FEA model because these do not represent the final design of the part in which generous fillets can be used at those areas to reduce stress concentrations. These areas can be analyzed later in more detail.

Figure 10 shows the meshing, the constraints, and the forces applied to the model. The female part was fixed in all directions on the face opposite to the connection. The male part was the one which moved to make contact against the female part, therefore, it could not be firmly fixed in all directions. Two truss elements were added to the male part to add stability in the vertical (Y) and horizontal (X) directions. The back face of the male part was fixed in the axial direction (Z) to stabilize it in that direction and to enable it to recover the reaction forces when full load was applied. The load was applied at the

male part as a tangential force with a value of one acting on a ring of nodes located on the outside perimeter of the part. This load was to be increased at every step according to the load vs. time line. The maximum value of 210 shown in the load vs time line is based on a maximum torque value of 400 ft-lb. Therefore, 210 x the number of nodes where the load is applied x the radial distance from the longitudinal axis = 400 ft-lb of torque.

Three different analyses with increasing degree of complexity were performed. All three analyses made use of the same load vs. time curve. The first run had contact elements at surfaces where contact was likely to occur. The surfaces located at each apex comprise three of those surfaces. The surfaces located immediately after the apex surfaces, in the direction of rotation due to the applied torque, comprise the other three. The friction between the two mating regions was not included in this first run. Thus, the solution time required was reduced, and the model validated; i.e., we could check for possible errors.

The second run included friction between the mating surfaces and calculation of the reaction forces at the back of the male part. The third run included friction between mating surfaces, reaction forces at the back of the male part and an angular velocity of 1047 rad/sec (10,000 rpm). The application angular velocity is also controlled by the time vs. load line. The angular velocity has to be scaled according to this line.

Discussion of results

Figures 11 through 14 show the maximum resultant displacement and maximum von Mises stresses acting on the female and male parts of the coupling for run number 1. As mentioned above, run number 1 did not specify any friction between the mating surfaces. The maximum displacements and stresses acting on the female part are 0.0015 in and about 40,000 psi respectively. The male part of the coupling showed maximum resultant displacements of 0.0112 in. and maximum von Mises stresses of 58,000 psi. The maximum von Mises stress of about 80,000 psi concentrated around the outside perimeter of the rear section of the male part must be disregarded. This

stress is due to the attachment of the truss elements that were added to help stabilize the model; therefore, they can be disregarded. The stresses are lower than the yield strength for 4340, which is 210,000 psi.

Figures 15 through 18 show the results obtained from run number 2. The maximum resultant displacements are 0.001 in and 0.011 in for the female and male parts respectively. The maximum von Mises stresses are 20,000 psi for both male and female parts. As can be seen, these stresses are one half the stresses obtained from run number 1. This difference should be expected because the addition of friction between the mating surfaces helps to convert some percentage of the energy that was creating tensile and shear stresses into creating traction forces. This helps in the transfer of loads from the male part to the female part. It also helps by dissipating concentrated loads over much larger areas, all of which results in lower stresses.

Run number 3, in which an angular velocity was added to the model, yielded results that were comparable to the results obtained from run number 2. Figures 19 and 20 show the maximum von Mises stresses and maximum resultant displacements acting on the male and female parts of the coupling respectively. Those two figures are almost identical to figures 16 and 17, which depict the maximum von Mises stresses and maximum resultant displacements for run number 2. This means that the loading due to the angular velocity is negligible.

The maximum displacement of 0.011 in obtained for all three analyses seems to be quite large if a rigid shaft is required. The reason for this is that the gap between male and female mating surfaces takes almost 0.008 in to close. This can be seen by examining figures 21 through 30. These figures depict the displacements and stresses of each one of the five time steps on run number 2. It should be noted that at step 3 in figure 23 no stress is seen in the mating area and that a resultant displacement of almost 0.008 in has already taken place. In the case of the real hardware, there is not supposed to be any gap between the mating surfaces; therefore, the displacements will be much smaller.

An additional analysis was performed to investigate the effects of the angular velocity on the female part of the coupling. A static analysis was performed on the female part with only centrifugal loading acting on it. Figures 31 and 32 show the von Mises stresses and resultant displacements for this case. The maximum von Mises stress is 1,600 psi and the maximum resultant displacements 0.0004 in, which make these stresses and displacements almost negligible when compared to the ones obtained due to the torque only.

Table 1 summarizes the results obtained on the three runs and includes the total time that it took to run every analysis. It can be seen that the third analysis took 18.24 hours of computer time to run on a Silicon Graphics® workstation. This time is different from real time. The third analysis took 2.5 days to run, which shows how lengthy this type of analysis is. Figures 31 and 32 show the displacements and stresses on female parts of coupling due to angular velocity.

It was essential to find out how much axial load would be generated by the application of a torque to the tapered polygon coupling because this information would be permitted knowing the amount of axial force that the tie bolt would have to withstand. Therefore, the reaction forces acting on the constrained nodes at the rear face of the male part of the coupling were printed to the output file of the analysis. Figure 33 shows a color plot of the reaction forces acting on the area mentioned above. It can be noted that the reaction forces are very low and will not have any effect on the behavior of the coupling.

Table 1. Results from the analyses

Run No.	Max. Resultant displacement @ step 5 female part (inches)	Max. resultant displacement @ step 5 male part (inches)	Max. mises stress @ step 5 female part (inches)	Max. mises stress @ step 5 male part (inches)	Run time (seconds)
1	0.0015	0.0112	40,000	58,000	25,059
2	0.001	0.011	20,000	20,000	60,309
3	0.001	0.011	20,000	20,000	65,648

Final remarks

This was not intended to be an in depth and final design and analysis of the multi-section shaft. There are some details that have to be worked out before the final design is reached. For instance, a fatigue analysis should be performed in order to investigate any long term problems related to this type of design. However, by examining the results obtained up to this point, it seems that the production of an eccentric shaft using this type of construction is feasible. The results show that the stresses are low and that the displacements are of no concern. The factor of safety based on minimum yield is a respectable 3.74 which is a very encouraging sign. They also show that the size of the tie bolt can be tailored more easily to comply with the lubrication requirements of the engine. Finally, the most important result obtained from the analysis is that the three-sided polygon coupling is a realistic option for the design of modular power trains.

Appendix

In the next pages we show the figures mentioned throughout the article.

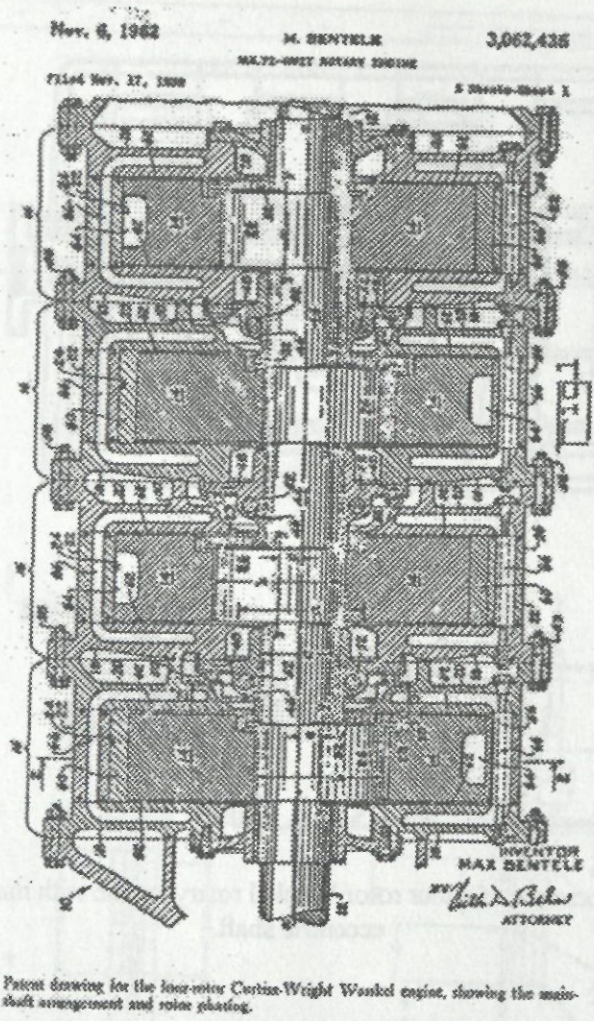

Patent drawing for the four-rotor Curtiss-Wright Wankel engine, showing the main-shaft arrangement and rotor phasing.

Figure 1. Example of a four rotor wankel engine with split stationary gears and main bearings

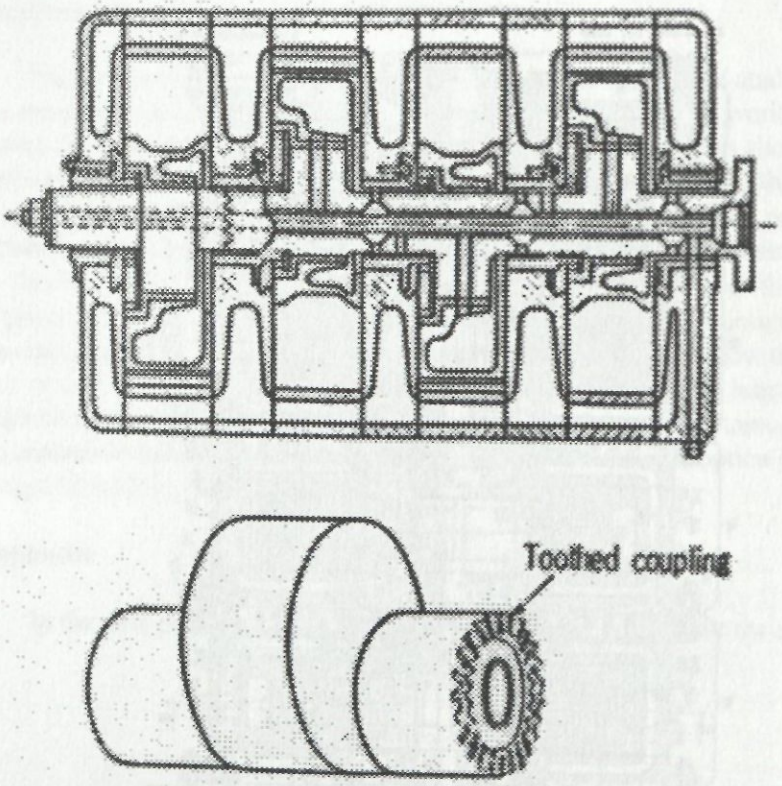

Figure 2. Example of a four rotor Wankel rotary engine with multi-section eccentric shaft

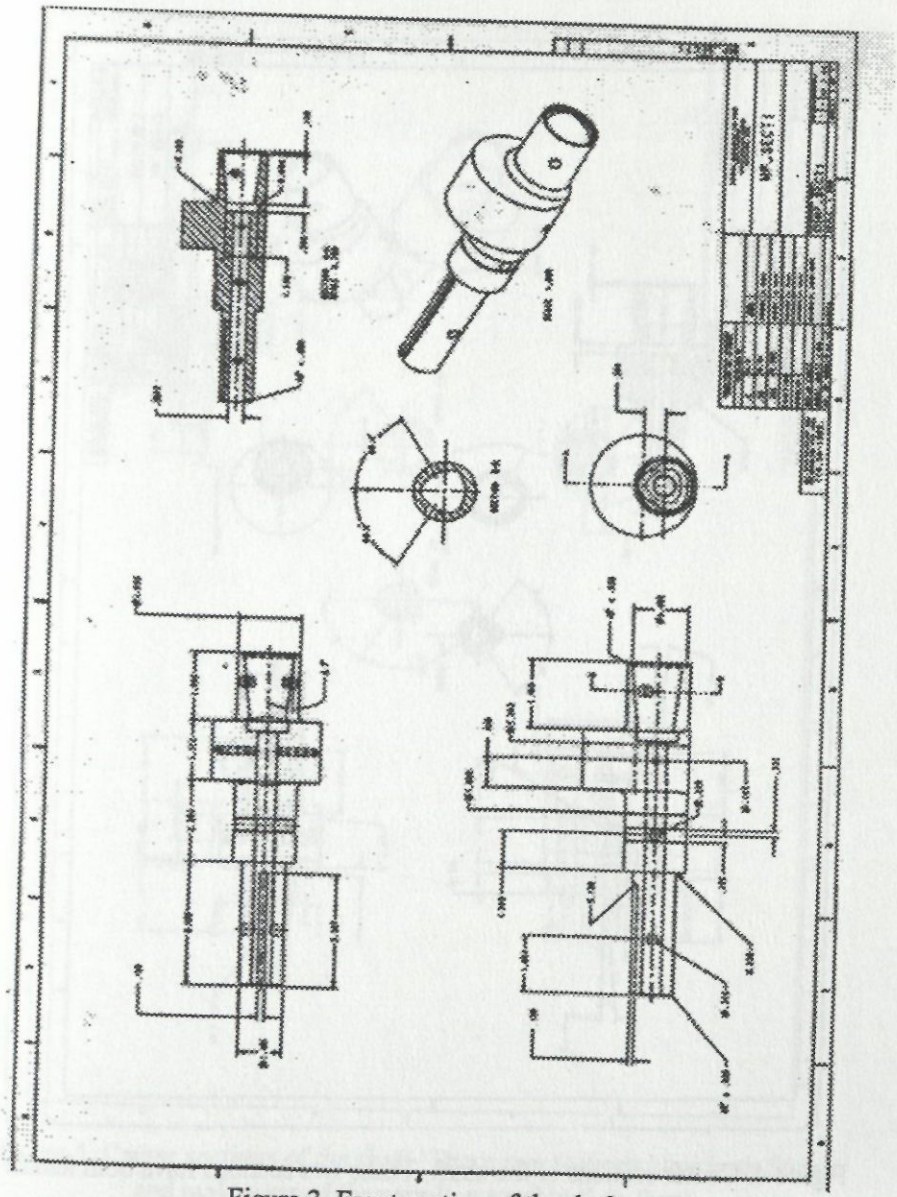

Figure 3. Front section of the shaft

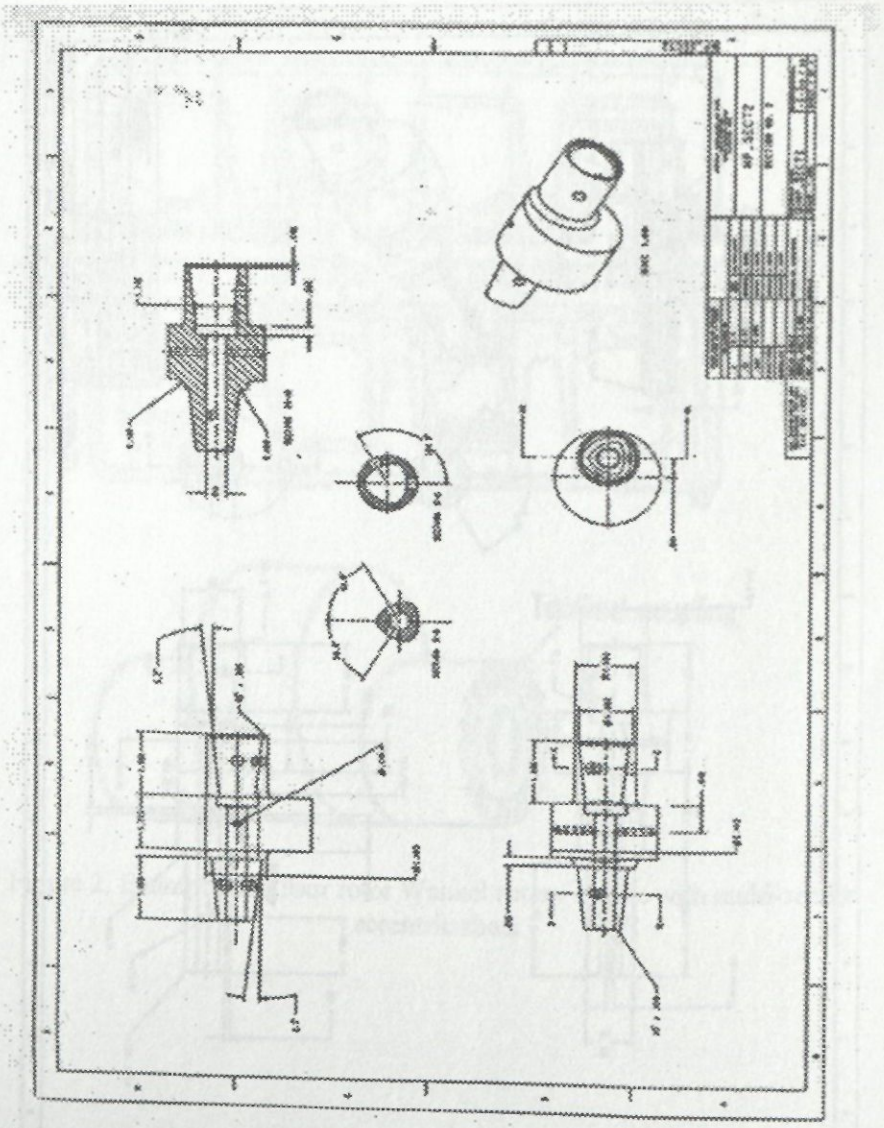

Figure 4. Center sections of the shaft. These two sections have both female and male parts of the coupling machined on them.

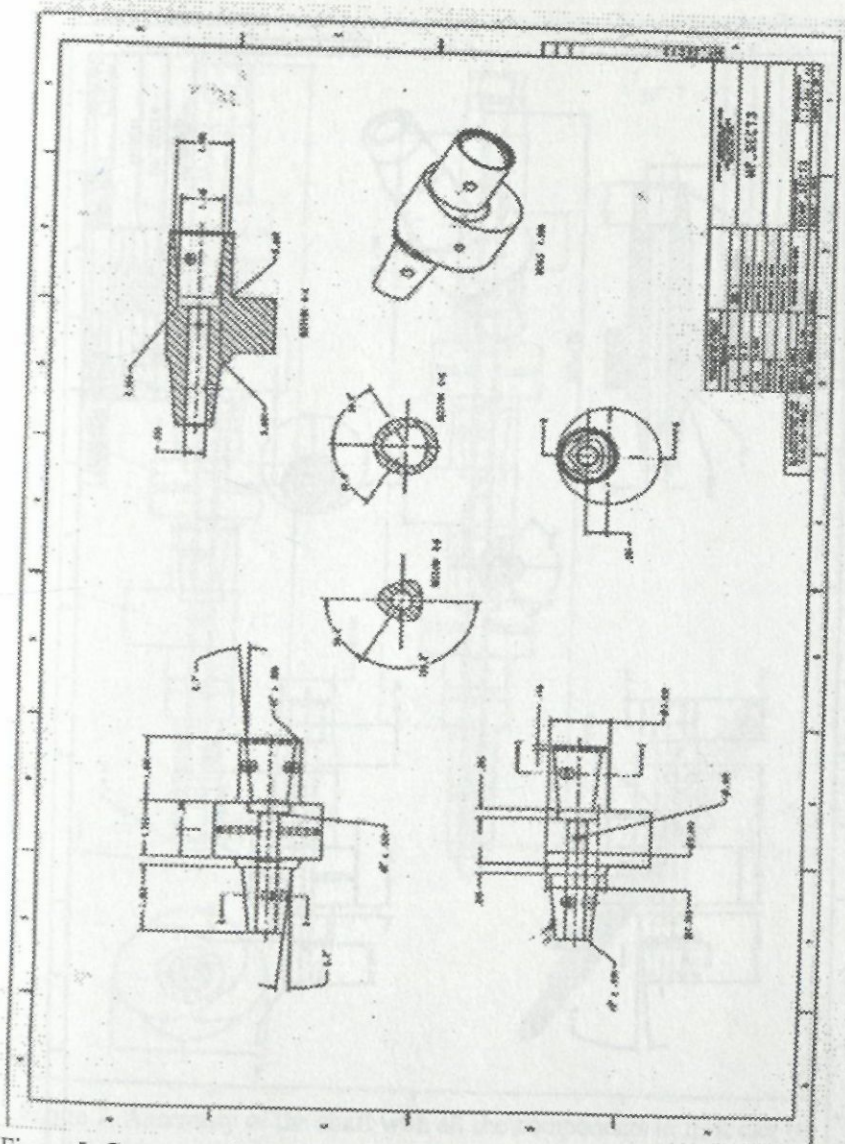

Figure 5. Center sections of the shaft. These two sections have both female and male parts of the coupling machined on them.

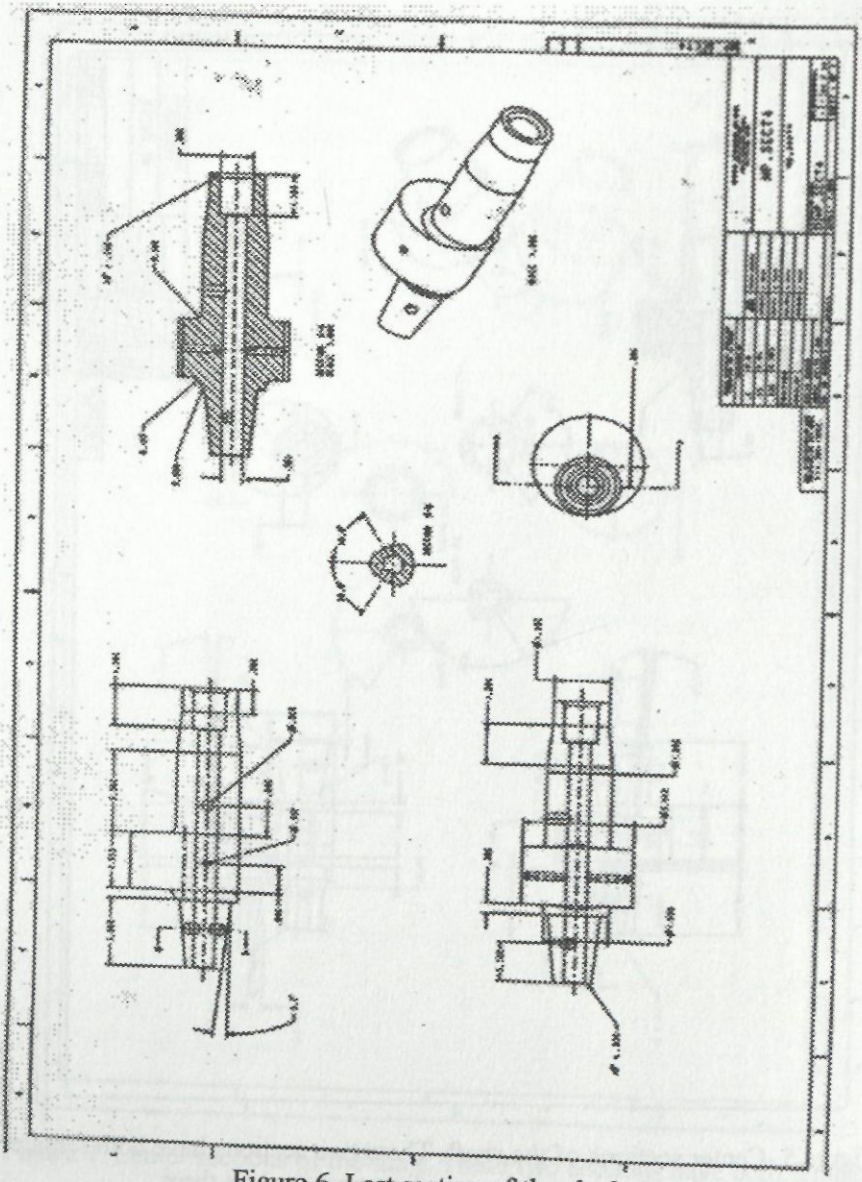

Figure 6. Last section of the shaft

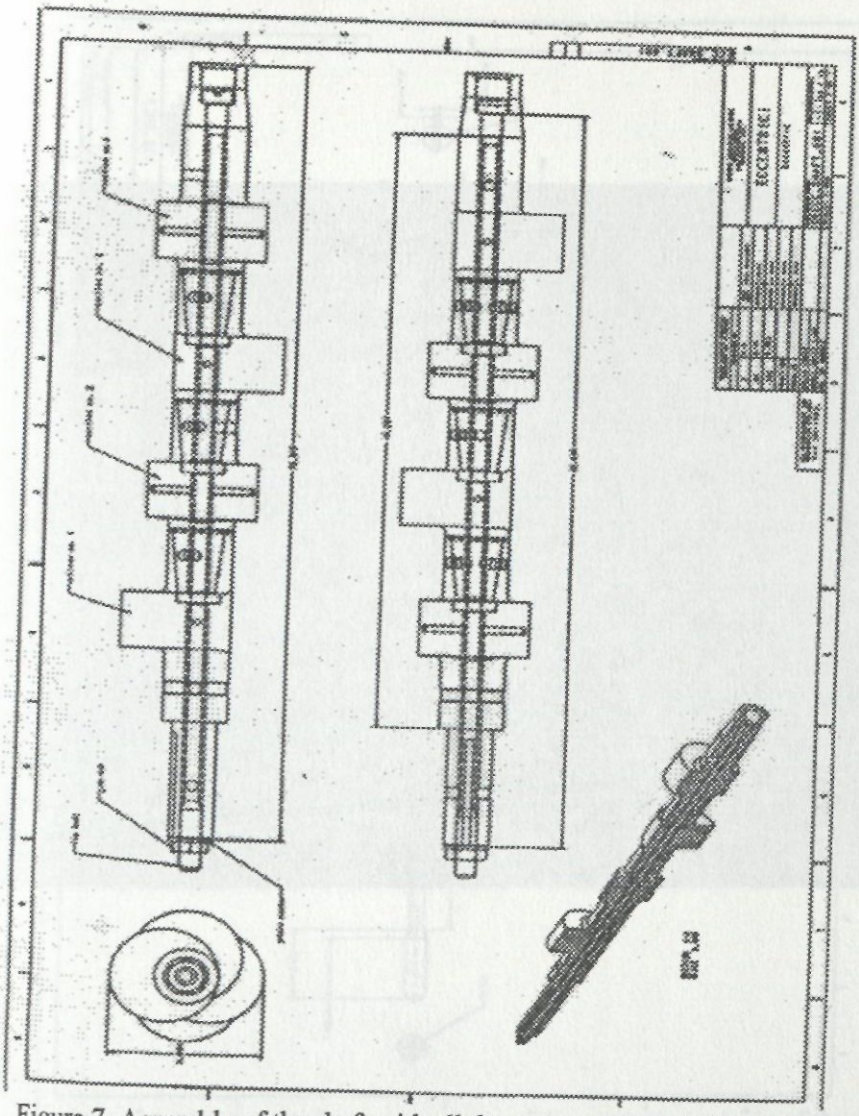

Figure 7. Assembly of the shaft with all the components in it. It can be noted that the eccentric sections are clocked 90 degrees clockwise from front to rear

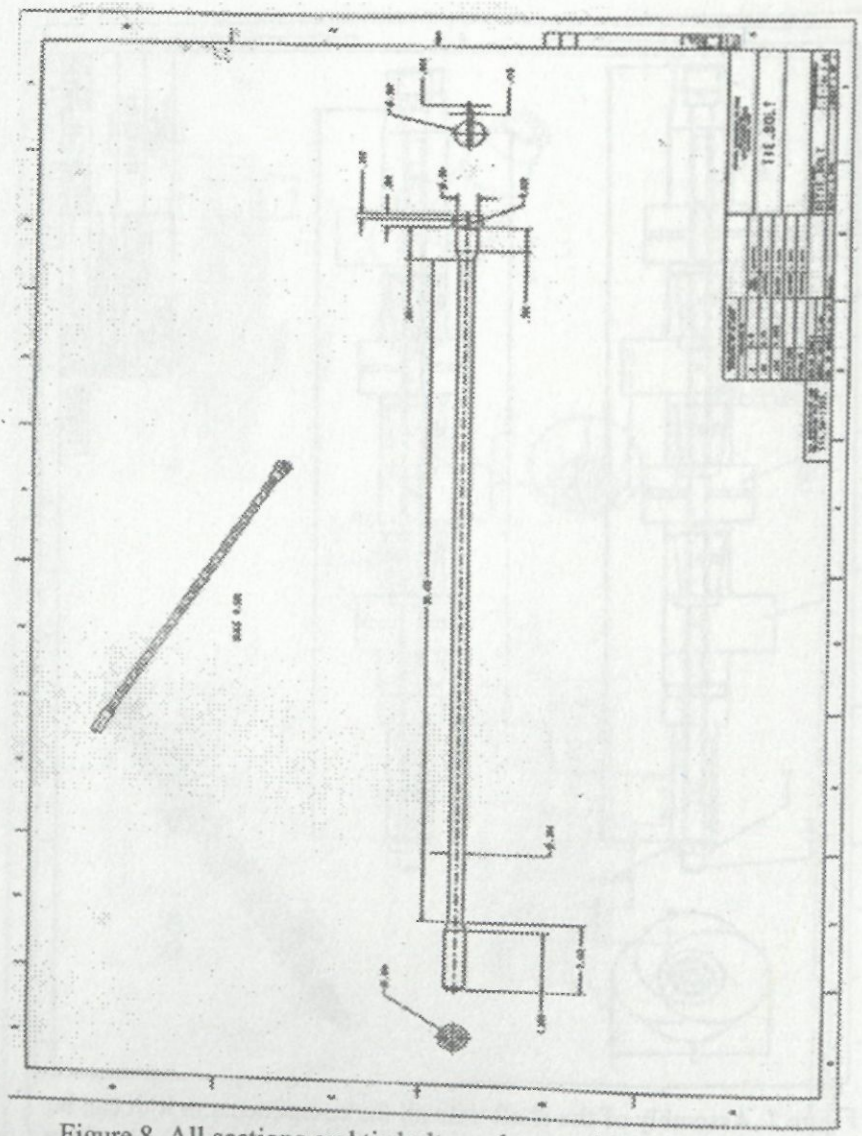

Figure 8. All sections and tie bolt, made out of 4340 low alloy steel forgings

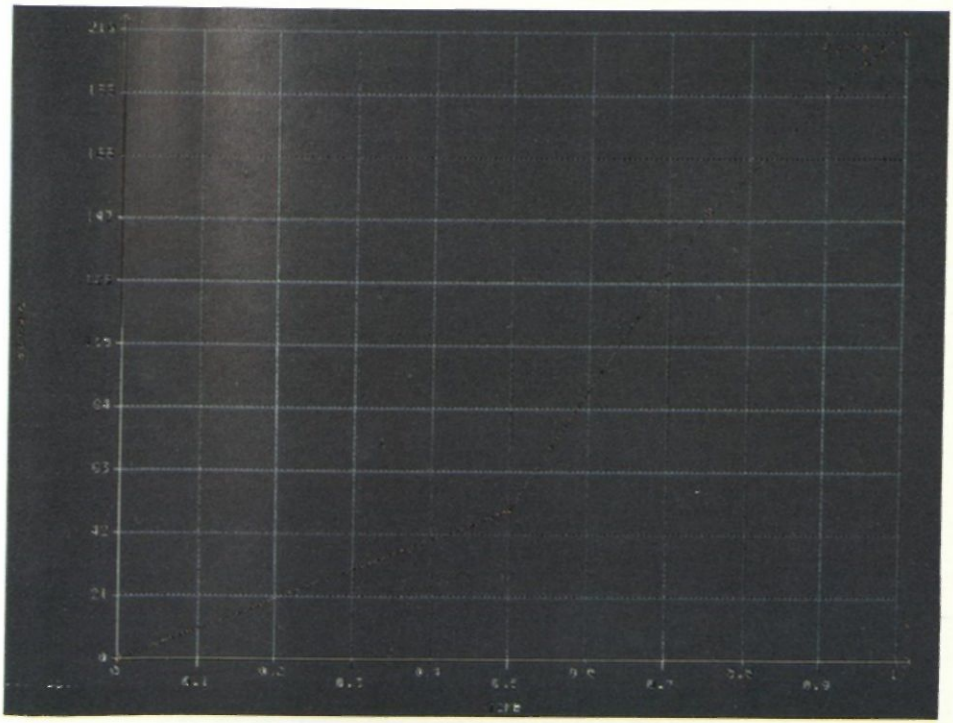

Figure 9. Load vs. time curve used on nonlinear static analysis of the polygon coupling. Value is the applied load (forces and angular velocities), time is given in seconds

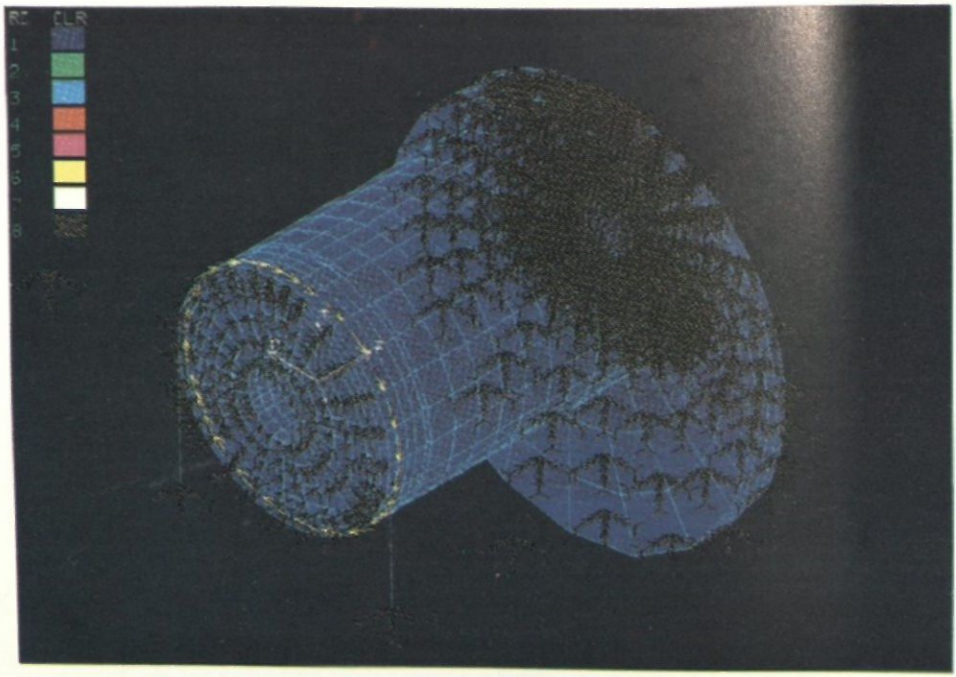

Figure 10. Finite element model of polygon connections with constraints and loads applied.

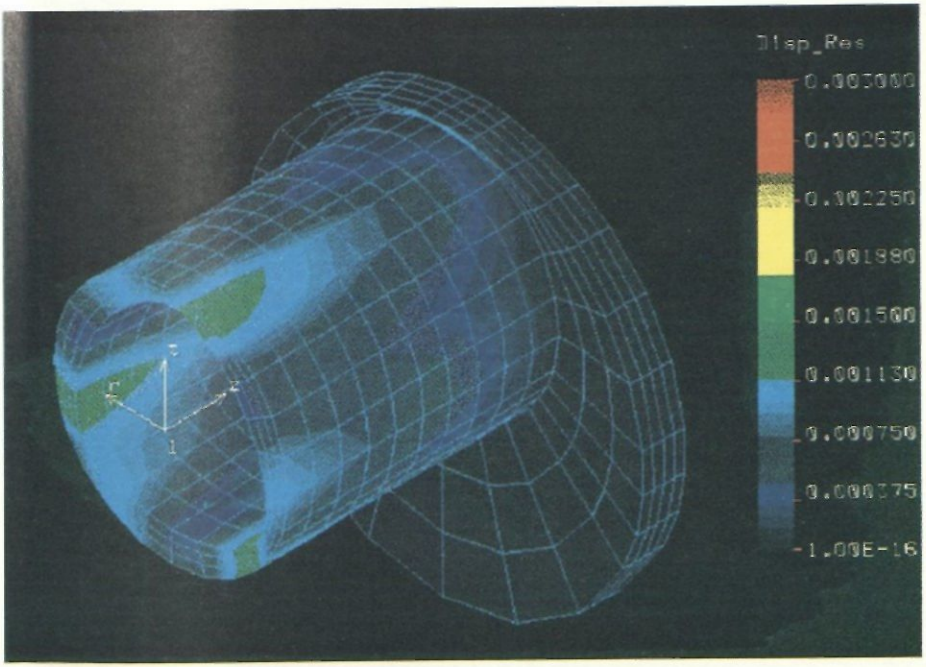

Figure 11 Maximum displacement on female part at step 5, no friction between mating parts, load applied=400 ft-lb of torque

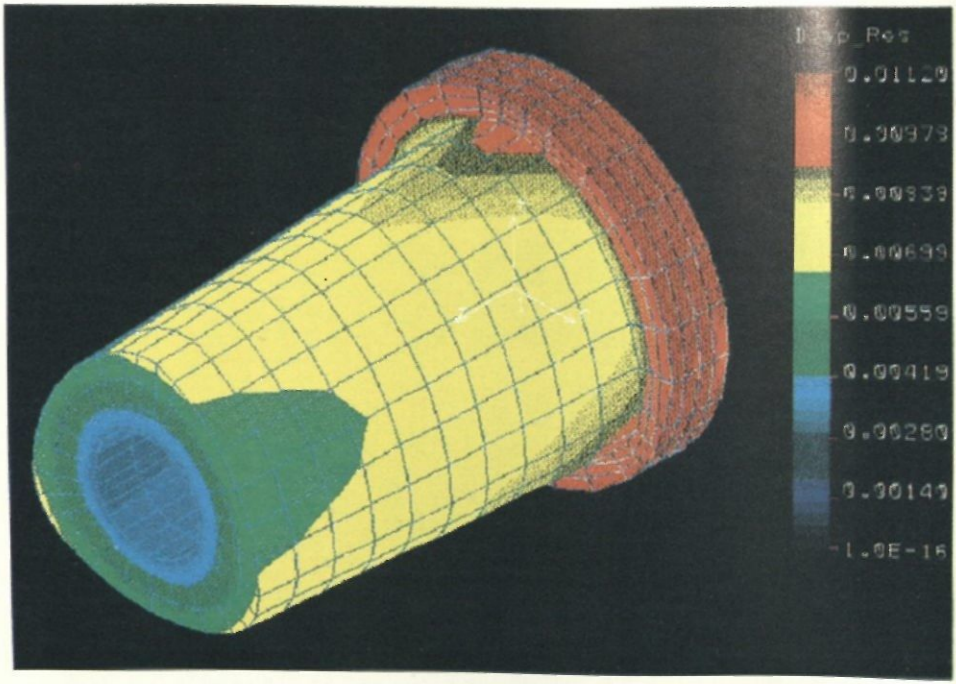

Figure 12 Maximum displacement on male part at step 5, no friction between mating parts, load applied=400 ft-lb of torque

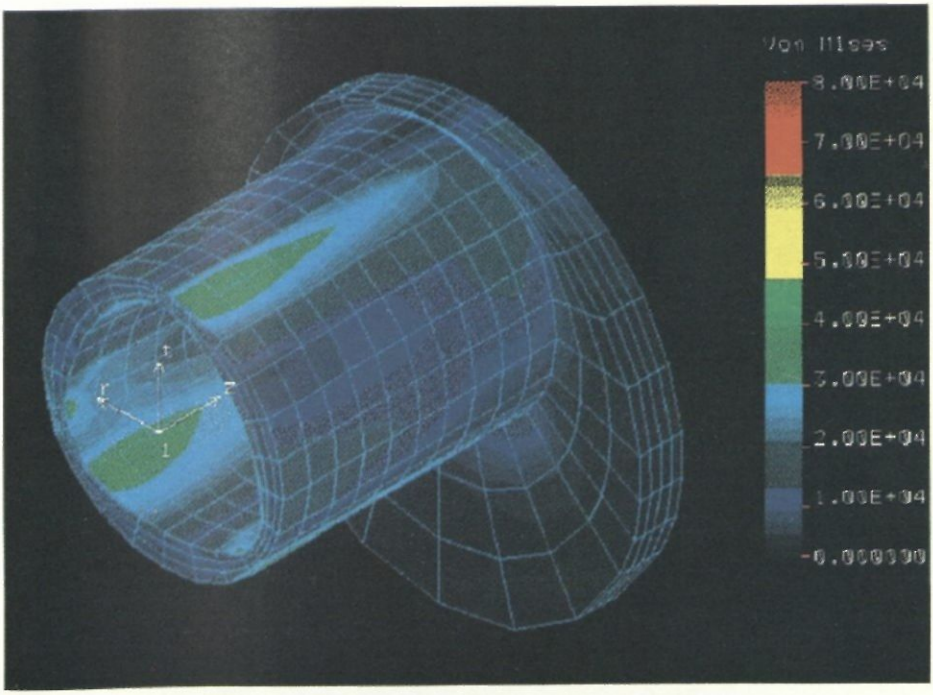

Figure 13 Maximum displacement on female part at step 5, no friction between mating parts, load applied=400 ft-lb of torque

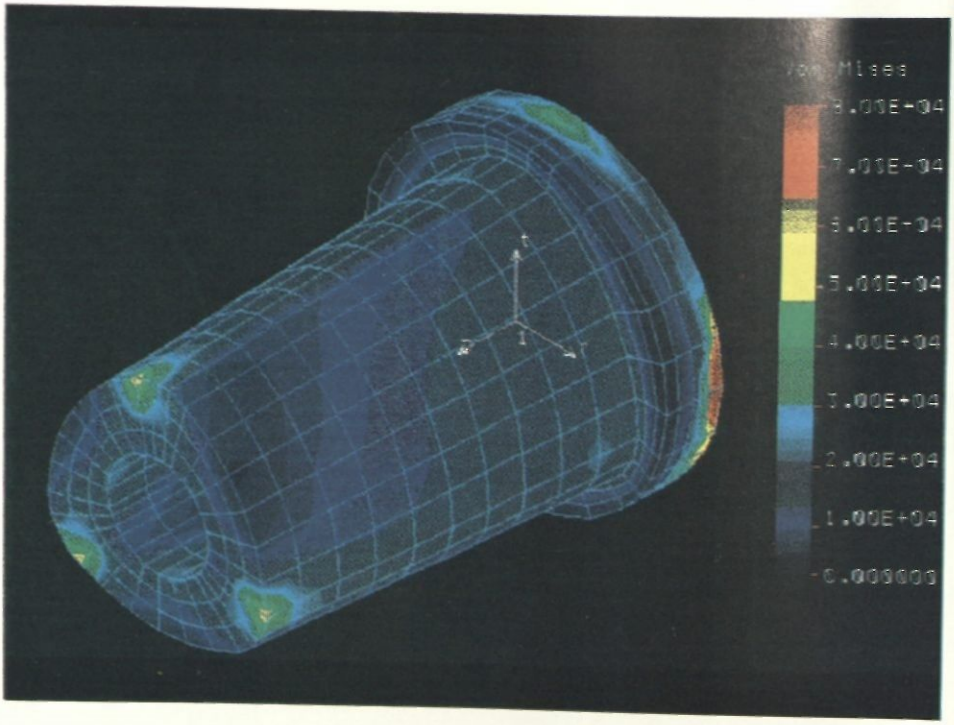

Figure 14 Maximum stresses on male part at step 5, no friction between mating parts, load applied=400 ft-lb of torque

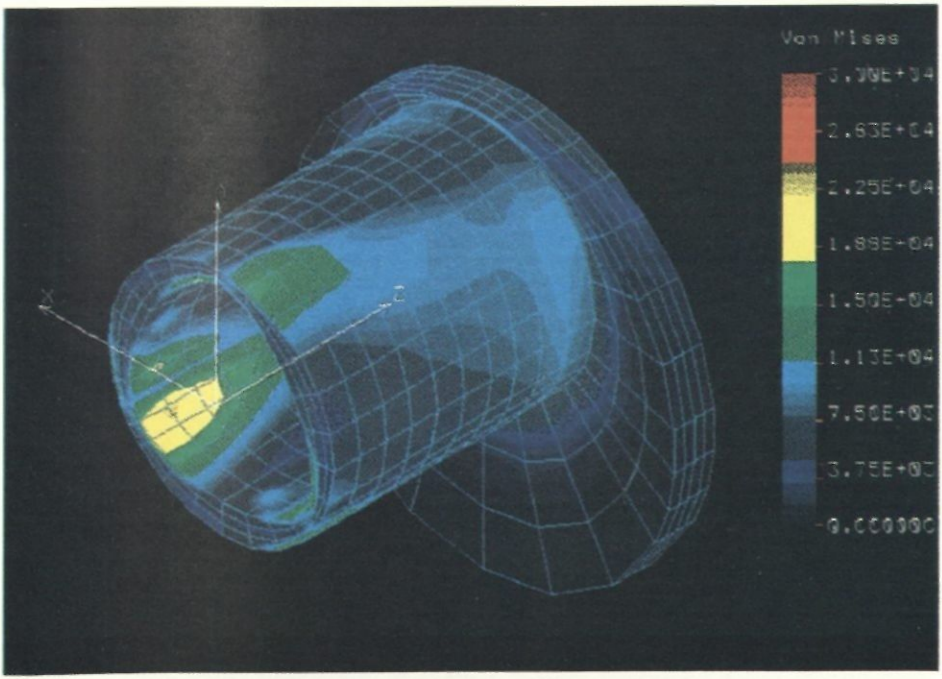

Figure 15 Stresses on female part at time step 5, friction between mating parts is included, load applied=400 ft-lb of torque

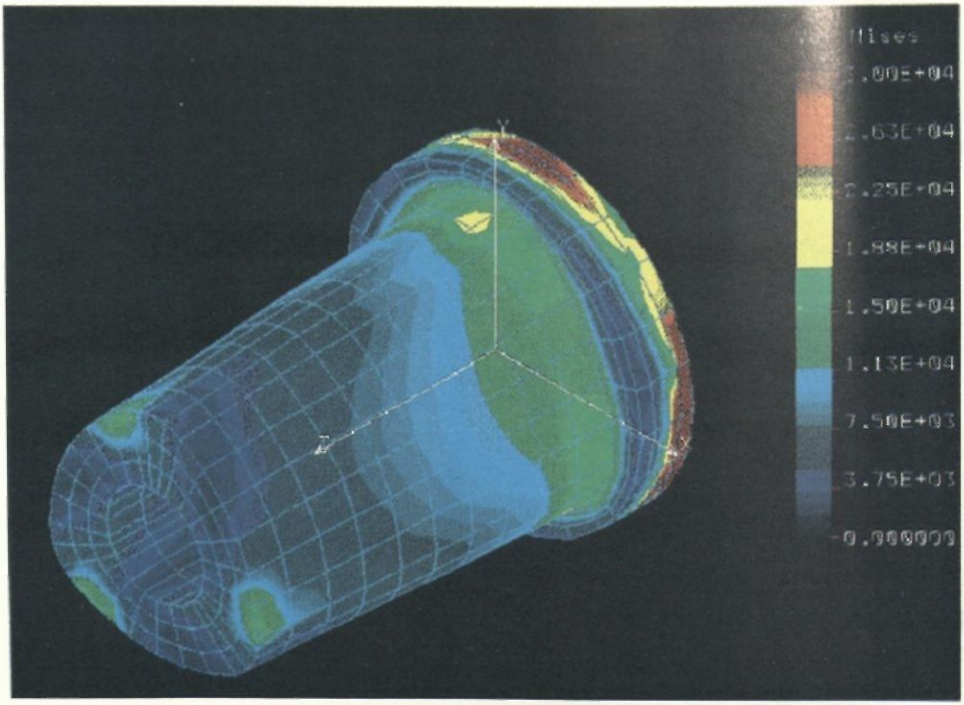

Figure 16 Stresses on male part at time step 5, friction between mating surfaces is included, load applied=400 ft-lb of torque

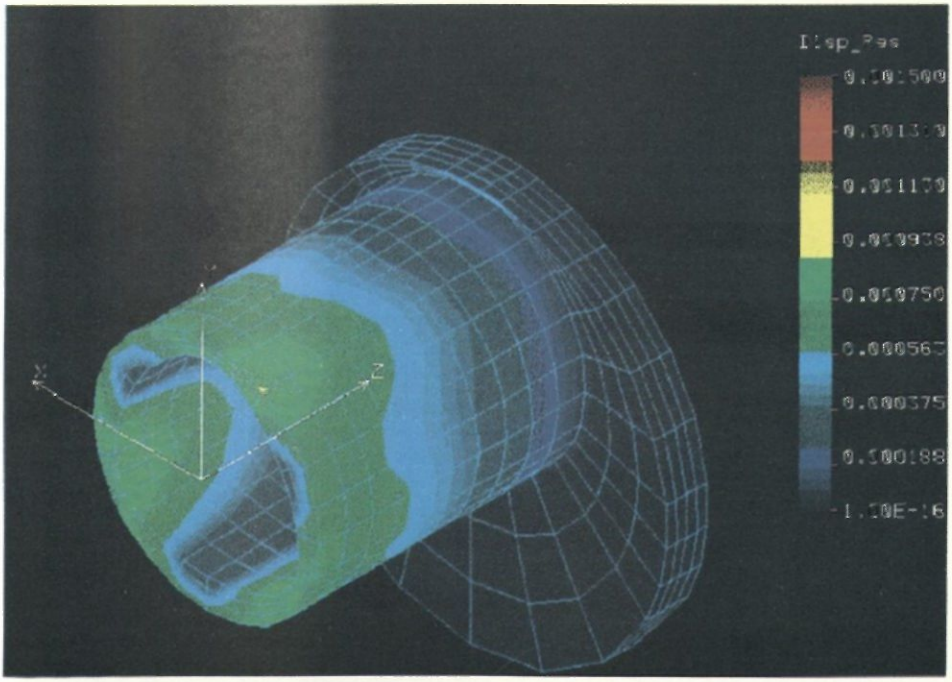

Figure 17. Displacements on female part at time step 5, friction between mating parts is included, load applied=400 ft-lb of torque

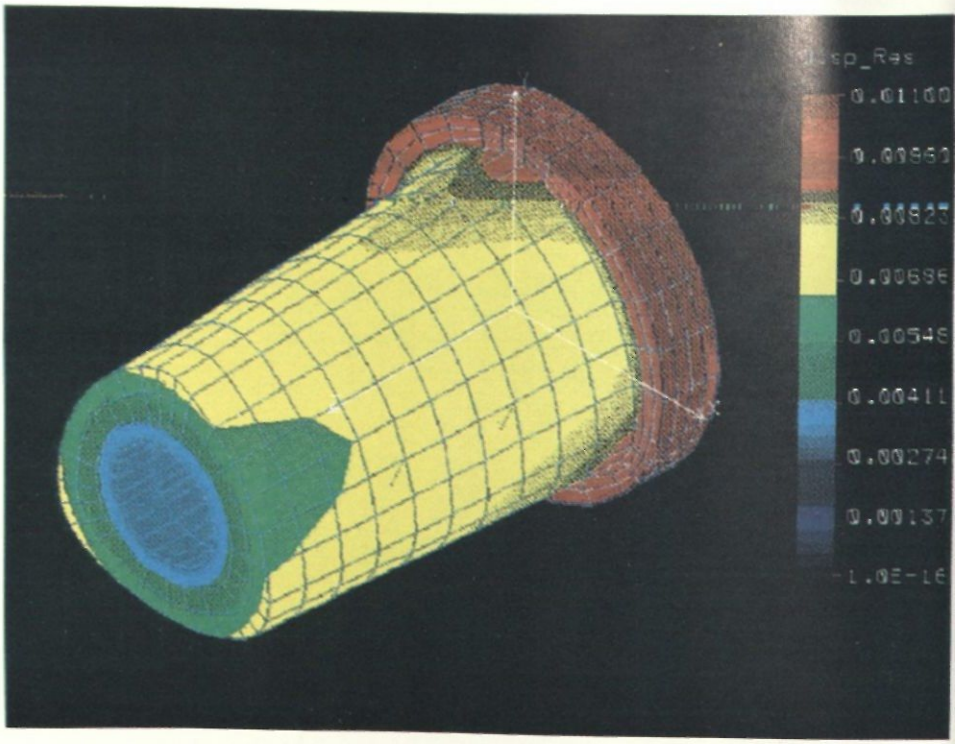

Figure 18. Displacements on male part at time step 5, friction between mating surfaces is included, load applied=400 ft-lb of torque

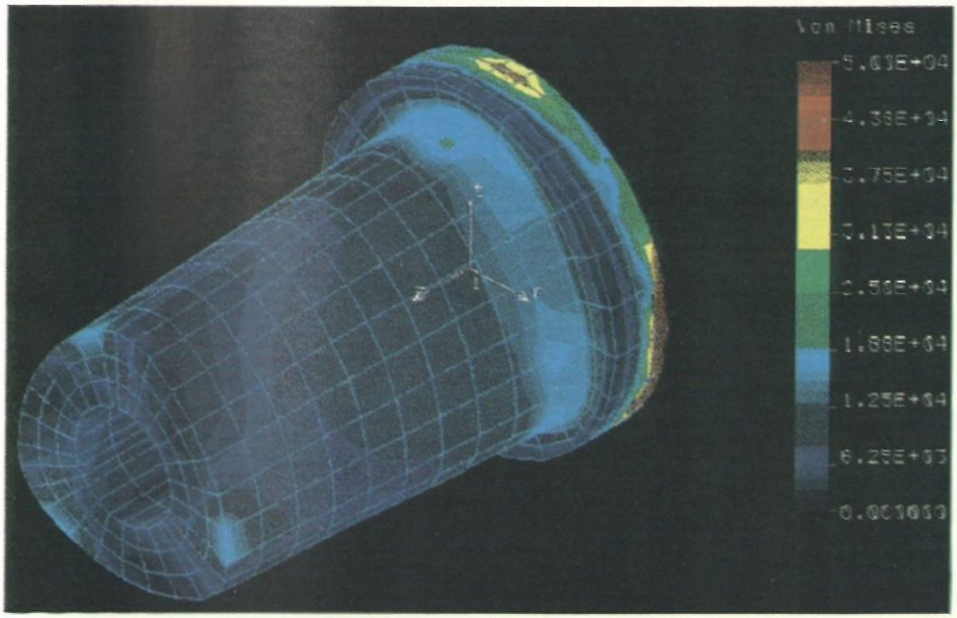

Figure 19. Stresses on male part at time step 5, friction between mating surfaces is included, load applied=400 ft-lb of torque, 10,000 RPM

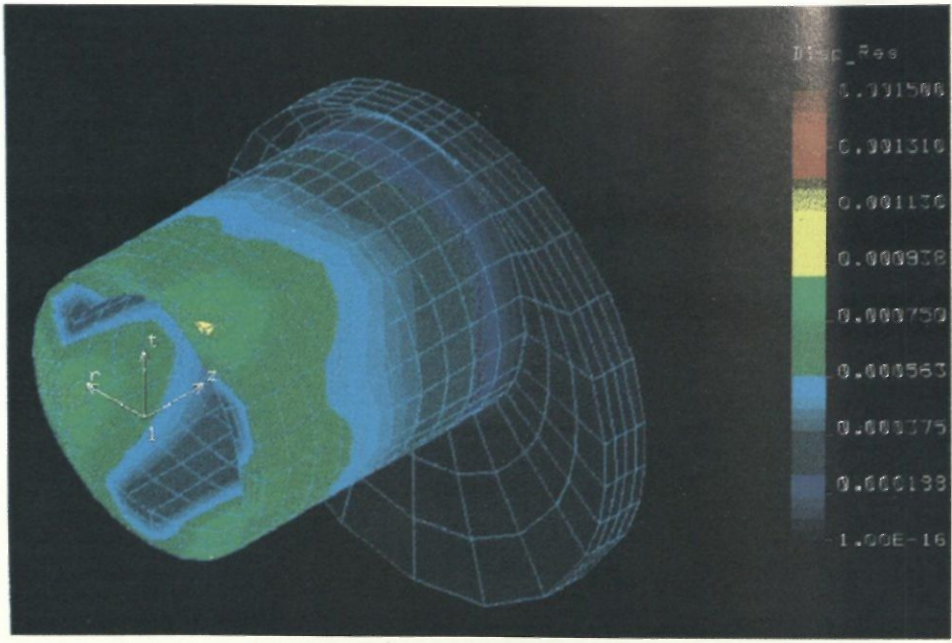

Figure 20. Stresses on female part at time step 5, friction between mating surfaces is included, load applied=400 ft-lb of torque, 10,000 RPM

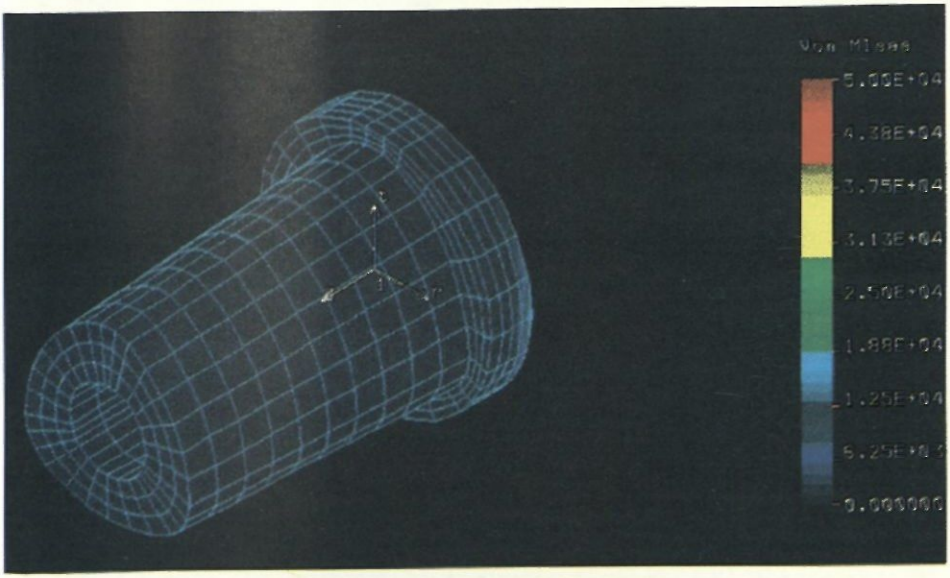

Figure 21. Stresses on male part at time step 1, friction between mating surfaces is included, load applied=400 ft-lb of torque.

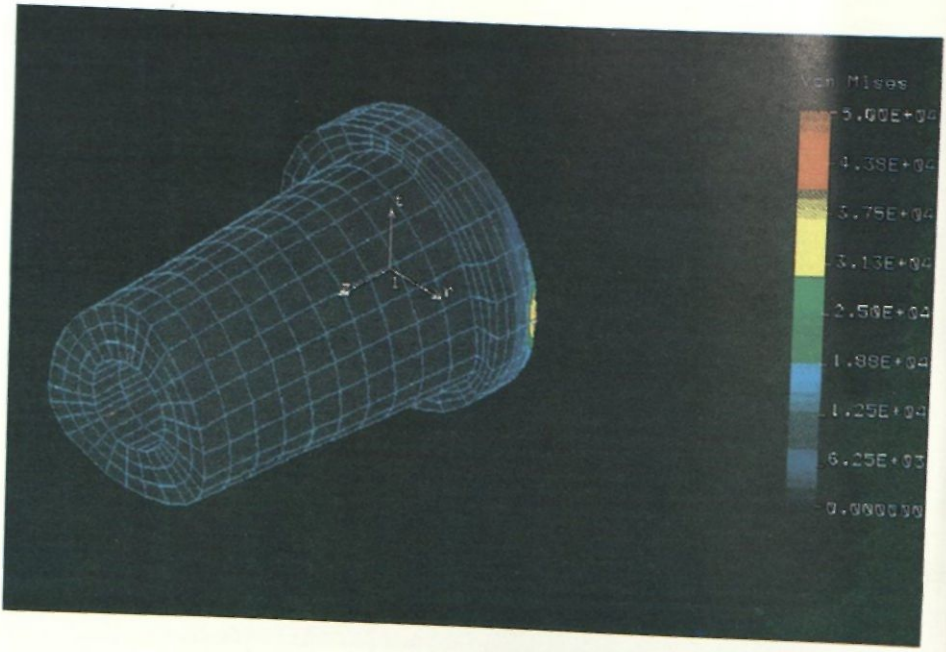

Figure 22. Stresses on male part at time step 2, friction between mating surfaces is included, load applied=400 ft-lb of torque.

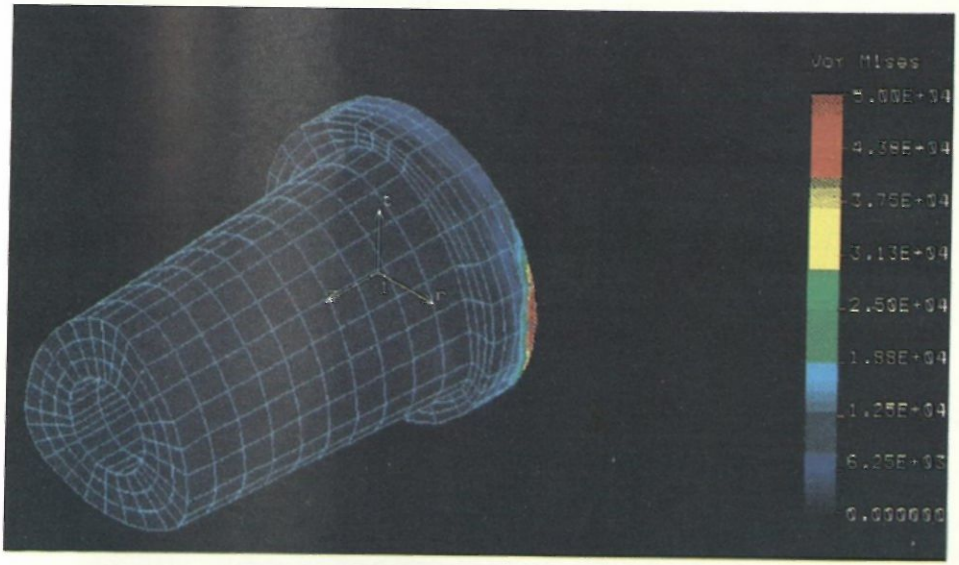

Figure 23. Stresses on male part at time step 3, friction between mating surfaces is included, load applied=400 ft-lb of torque.

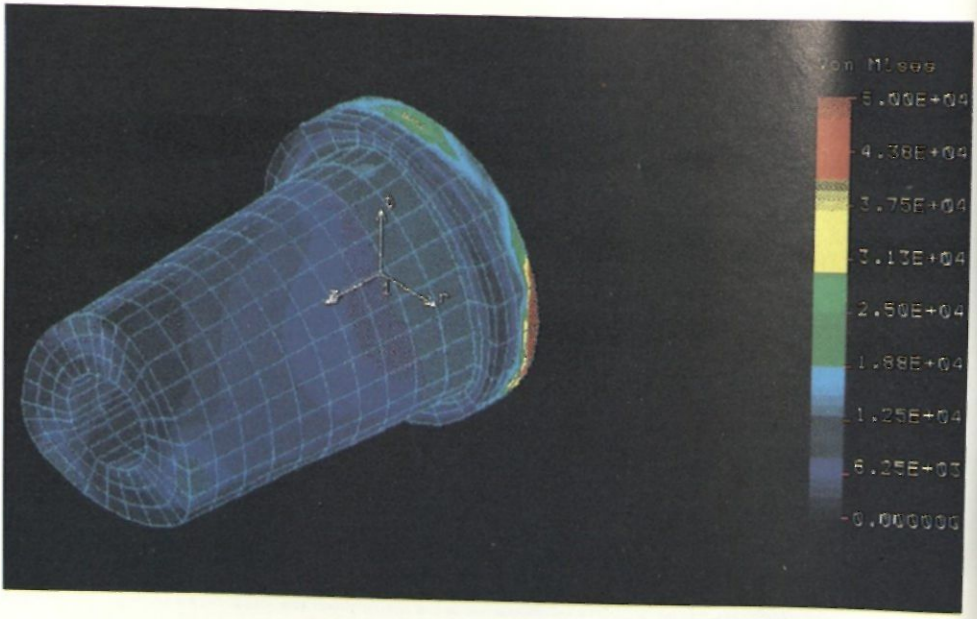

Figure 24. Stresses on male part at time step 4, friction between mating surfaces is included, load applied=400 ft-lb of torque.

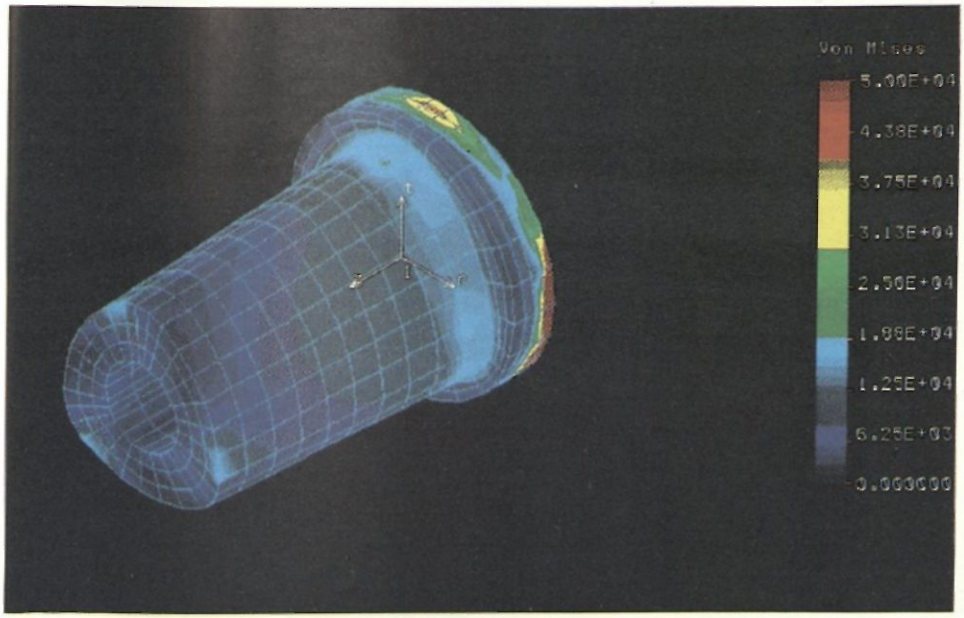

Figure 25. Stresses on male part at time step 5, friction between mating surfaces is included, load applied=400 ft-lb of torque, 10,000 RPM

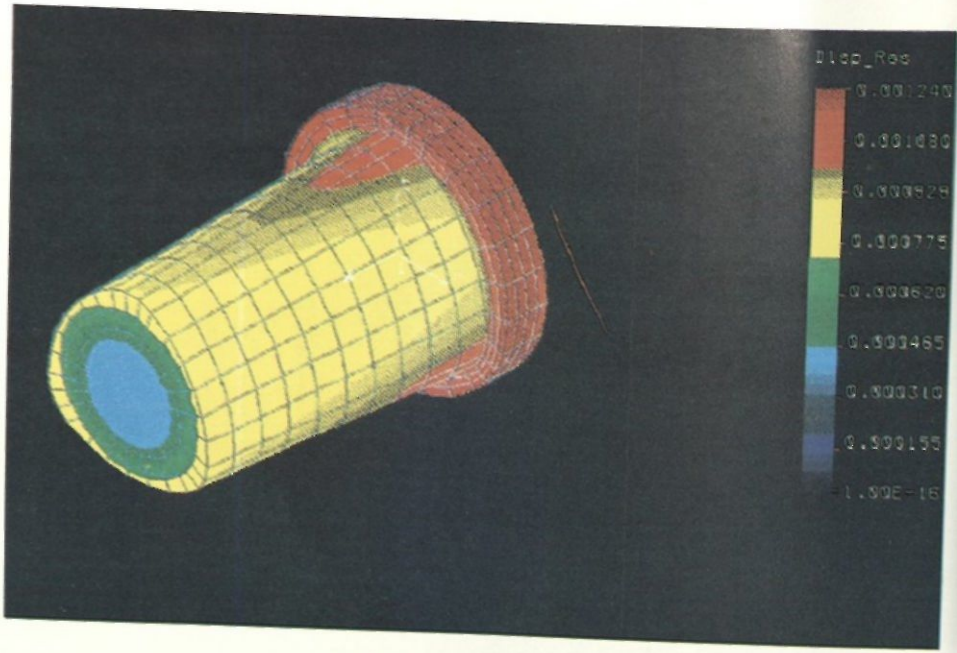

Figure 26. Displacements on male part at time step 1, friction between mating surfaces is included, load applied=400 ft-lb of torque.

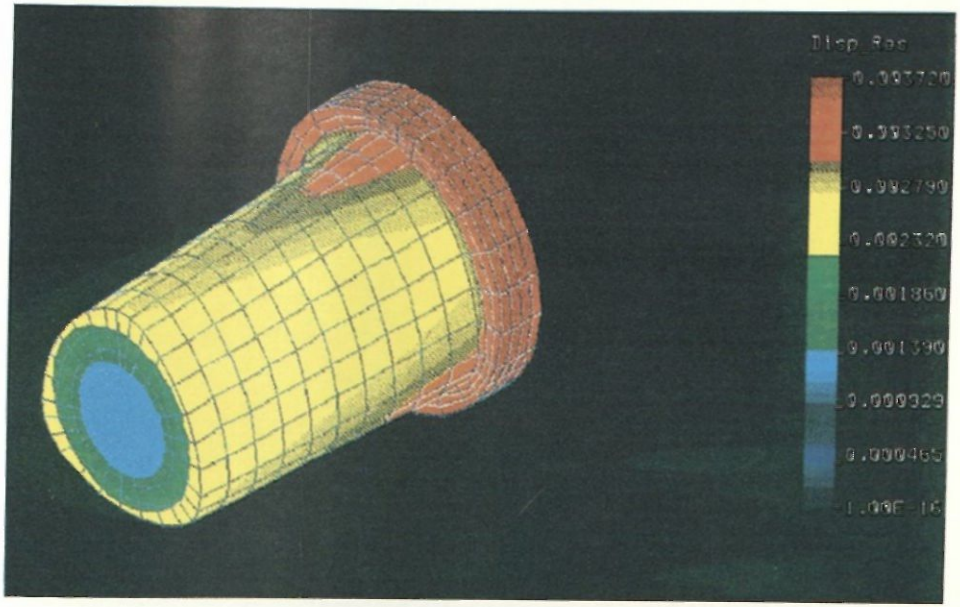

Figure 27. Displacements on male part at time step 2, friction between mating surfaces is included, load applied=400 ft-lb of torque.

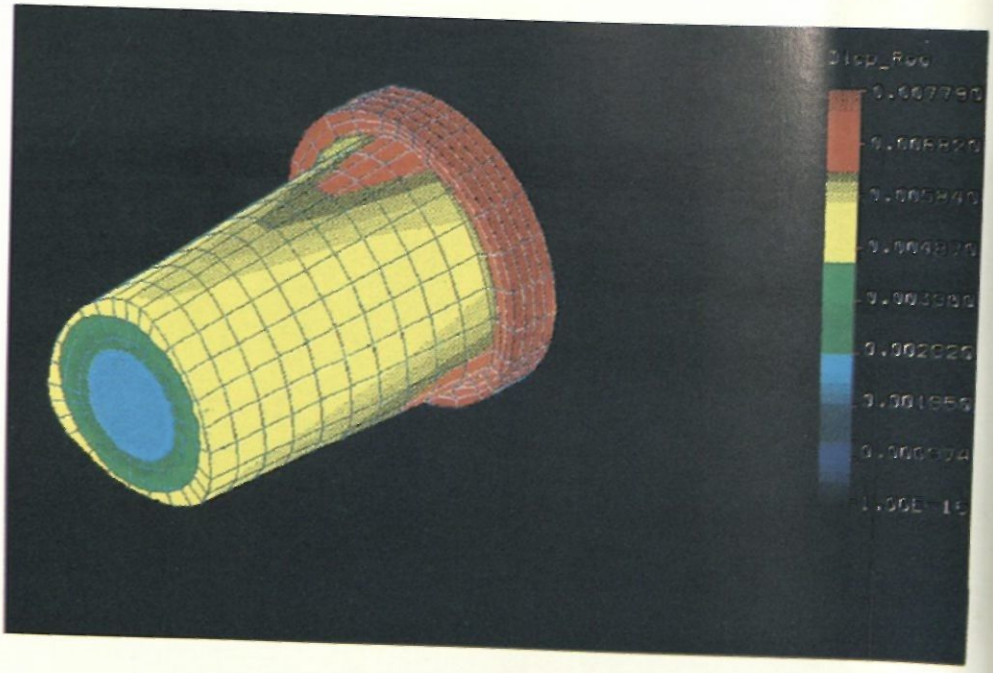

Figure 28. Displacements on male part at time step 3, friction between mating surfaces is included, load applied=400 ft-lb of torque.

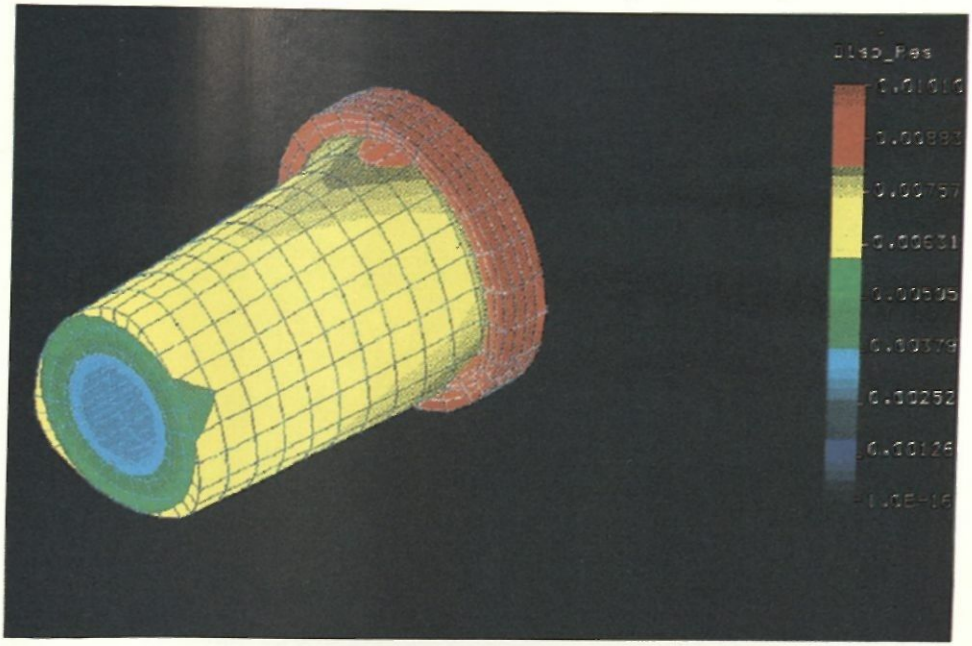

Figure 29. Displacements on male part at time step 4, friction between mating surfaces is included, load applied=400 ft-lb of torque.

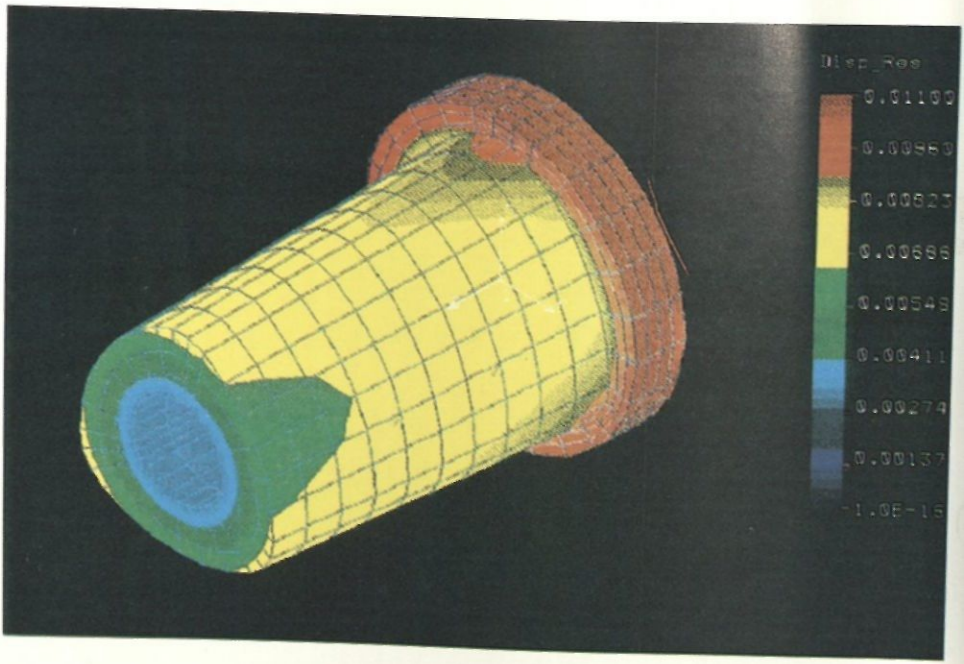

Figure 30. Displacements on male part at time step 5, friction between mating surfaces is included, load applied=400 ft-lb of torque.

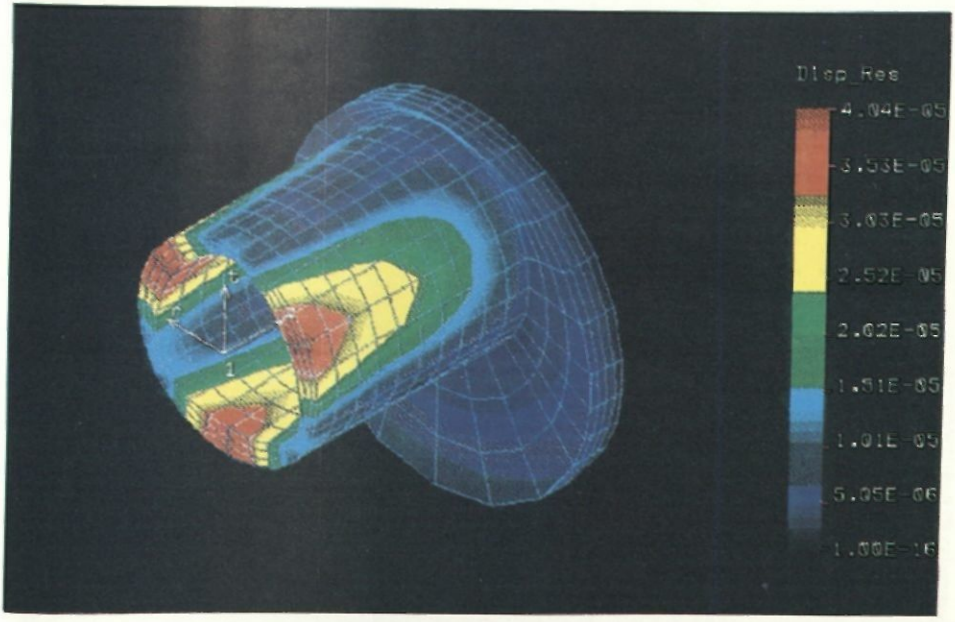

Figure 31. Displacements on female part due to centrifugal load. This load is 1047 rad/sec (10,000 RPM)

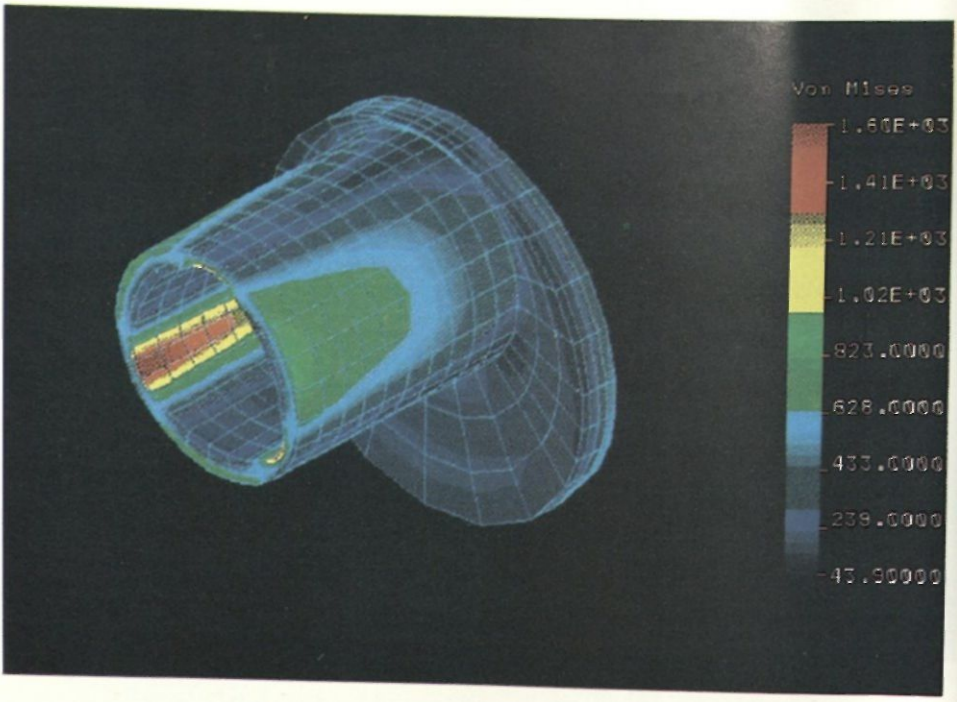

Figure 32. Stresses on female part due to centrifugal load. This load is 1047 rad/sec (10,000 RPM)

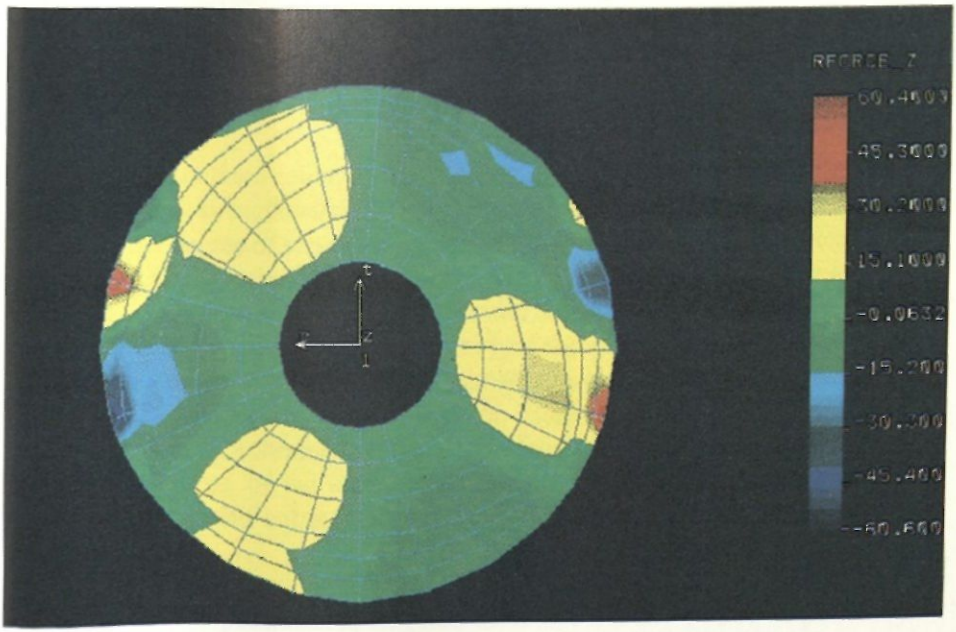

Figure 33. Reaction force in the axial direction (z), friction between mating surfaces is included, load applied=400 ft-lb of torque.